



Relationship between neuromelanin and dopamine terminals within the Parkinson's nigrostriatal system

Antonio Martín-Bastida,^{1,2,*}  Nicholas P. Lao-Kaim,^{1,*} Andreas Antonios Roussakis,¹ Graham E. Searle,³ Yue Xing,⁴ Roger N. Gunn,^{3,5} Stefan T. Schwarz,⁴ Roger A. Barker,⁶ Dorothee P. Auer⁴ and  Paola Piccini¹

*These authors contributed equally to this work.

Parkinson's disease is characterized by the progressive loss of pigmented dopaminergic neurons in the substantia nigra and associated striatal deafferentation. Neuromelanin content is thought to reflect the loss of pigmented neurons, but available data characterizing its relationship with striatal dopaminergic integrity are not comprehensive or consistent, and predominantly involve heterogeneous samples. In this cross-sectional study, we used neuromelanin-sensitive MRI and the highly specific dopamine transporter PET radioligand, ¹¹C-PE2I, to assess the association between neuromelanin-containing cell levels in the substantia nigra pars compacta and nigrostriatal terminal density *in vivo*, in 30 patients with bilateral Parkinson's disease. Fifteen healthy control subjects also underwent neuromelanin-sensitive imaging. We used a novel approach taking into account the anatomical and functional subdivision of substantia nigra into dorsal and ventral tiers and striatal nuclei into pre- and post-commissural subregions, in accordance with previous animal and post-mortem studies, and consider the clinically asymmetric disease presentation. *In vivo*, Parkinson's disease subjects displayed reduced neuromelanin levels in the ventral ($-30 \pm 28\%$) and dorsal tiers ($-21 \pm 24\%$) as compared to the control group [$F(1,43) = 11.95$, $P = 0.001$]. Within the Parkinson's disease group, nigral pigmentation was lower in the ventral tier as compared to the dorsal tier [$F(1,29) = 36.19$, $P < 0.001$] and lower in the clinically-defined most affected side [$F(1,29) = 4.85$, $P = 0.036$]. Similarly, lower dopamine transporter density was observed in the ventral tier [$F(1,29) = 76.39$, $P < 0.001$] and clinically-defined most affected side [$F(1,29) = 4.21$, $P = 0.049$]. Despite similar patterns, regression analysis showed no significant association between nigral pigmentation and nigral dopamine transporter density. However, for the clinically-defined most affected side, significant relationships were observed between pigmentation of the ventral nigral tier with striatal dopamine transporter binding in pre-commissural and post-commissural striatal subregions known to receive nigrostriatal projections from this tier, while the dorsal tier correlated with striatal projection sites in the pre-commissural striatum ($P < 0.05$, Benjamini-Hochberg corrected). In contrast, there were no statistically significant relationships between these two measures in the clinically-defined least affected side. These findings provide important insights into the topography of nigrostriatal neurodegeneration in Parkinson's disease, indicating that the characteristics of disease progression may fundamentally differ across hemispheres and support post-mortem data showing asynchrony in the loss of neuromelanin-containing versus tyrosine hydroxylase positive nigral cells.

- 1 Centre for Neuroinflammation and Neurodegeneration, Division of Brain Sciences, Imperial College London, London, W12 0NN, UK
- 2 Neurology Department, Clinica Universidad de Navarra, Pamplona, Navarra, 31008, Spain
- 3 Invicro LLC, London, UK
- 4 Radiological Sciences, Division of Clinical Neuroscience, University of Nottingham, Queen's Medical Centre, Nottingham NG7 2UH, UK

- 5 Centre for Restorative Neuroscience, Centre for Neuroinflammation and Neurodegeneration, Division of Brain Sciences, Imperial College London, London, W12 0NN, UK
 6 John Van Geest Centre for Brain Repair, University of Cambridge, Cambridge CB2 0PY, UK

Correspondence to: Paola Piccini

Neurology Imaging Unit, Centre for Neuroinflammation and Neurodegeneration, Division of Brain Sciences, Imperial College London, London, W12 0NN, UK
 E-mail: paola.piccini@imperial.ac.uk

Keywords: Parkinson's disease; magnetic resonance imaging; positron emission tomography; neuromelanin; dopamine transporter

Abbreviations: DAT = dopamine transporter; SNc = substantia nigra pars compacta; SNc^{dor} = substantia nigra pars compacta dorsal tier; SNc^{ven} = substantia nigra pars compacta ventral tier; UPDRS-III = Unified Parkinson's Disease Rating Scale part III

Introduction

The main pathological hallmarks of Parkinson's disease consist of the progressive loss of pigmented dopaminergic neurons in the substantia nigra pars compacta (SNc) and a reduction of dopaminergic striatal afferents (Fearnley and Lees, 1991). An important factor in the disease aetiology concerns the function of neuromelanin that is contained within pigmented SNc neurons. Neuromelanin is a dark insoluble complex compound that is synthesized as a byproduct of dopamine oxidation during cytosolic dopamine homeostasis. Physiologically, neuromelanin is proposed to have a dual role. It sequesters potentially toxic organic chemical, exogenous and endogenous metals such as iron in redox-inactive state while its synthesis confers neuroprotection from cytosolic reactive or toxic quinones. However, neuromelanin released into the extracellular space upon neuronal death, as is the case in Parkinson's disease, further exacerbates neurodegeneration by releasing toxic metals and catecholaminergic products and inducing oxidative stress, local microglial activation and chronic inflammation (Zecca *et al.*, 2006; Zucca *et al.*, 2014, 2017).

Neuromelanin bound to metals such as iron and copper is highly paramagnetic, leading to T₁-shortening and hyperintense signal on T₁-weighted turbo spin-echo (TSE) MRI sequences (Sulzer *et al.*, 2018). Hyperintensity in such images demonstrates direct associations with post-mortem neuromelanin-containing dopaminergic cell counts (Kitao *et al.*, 2013). In recent years several studies evaluating nigral depigmentation have demonstrated the ability for neuromelanin-sensitive MRI to distinguish between Parkinson's disease and healthy individuals with high sensitivity and specificity, representing a potential *in vivo* index of neuromelanin content, disease progression and nigral cell death (Sasaki *et al.*, 2006; Kashiwara *et al.*, 2011; Schwarz *et al.*, 2011; Matsuura *et al.*, 2013; Ogisu *et al.*, 2013; Ohtsuka *et al.*, 2013; Castellanos *et al.*, 2015; Reimao *et al.*, 2015; Fabbri *et al.*, 2017).

Overall estimations suggest that ~30% of neuromelanin-containing cells in the SNc are lost prior to the appearance of classical Parkinson's disease motor symptoms (Fearnley and Lees, 1991; Cheng *et al.*, 2010). In contrast, depletion of dopaminergic terminal markers in the principal

projection sites of the striatum is in most cases much more pronounced at symptomatic threshold. Typically deficits of striatal dopamine integrity are estimated between 50–80% as compared to control subjects, although lower values of ~20% have been reported (Bernheimer *et al.*, 1973; Nyberg *et al.*, 1983; Kish *et al.*, 1988; Scherman *et al.*, 1989; Lee *et al.*, 2000; Cheng *et al.*, 2010). The difference between these estimates raises questions regarding the relationship between neuromelanin and the integrity of nigrostriatal terminals.

To date, three studies have examined pigmented cell density in the SNc at post-mortem, alongside striatal dopamine transporter (DAT) binding measured *in vivo* with ¹²³I-FP-CIT [N-(3-fluoropropyl)-2β-carbomethoxy-3β-(4-[¹²³I]iodophenyl)nortropane] single photon emission computed tomography (SPECT) at 2.5–5 years ante-mortem, but with conflicting results (Colloby *et al.*, 2012; Kraemmer *et al.*, 2014; Saari *et al.*, 2017). Nigral cell counts were related to ¹²³I-FP-CIT striatal specific binding ratios in Parkinson's disease dementia (Colloby *et al.*, 2012) and heterogeneous neurological (Kraemmer *et al.*, 2014) samples. This correlation was not present in a small group of 11 patients with Parkinson's disease (Saari *et al.*, 2017), leading Saari and colleagues to hypothesize that the relationship between surviving nigral cells and striatal dopamine is lost in later stages of the disease. To our knowledge, only two recent studies have assessed this relationship in a multimodal setting. Using neuromelanin-sensitive MRI, strong positive correlations were demonstrated between striatal DAT binding and both substantia nigra volume, as well as the substantia nigra-to-cerebral peduncle contrast ratios, in cohorts with idiopathic Parkinson's disease (Isaias *et al.*, 2016) and mixed parkinsonism (Kuya *et al.*, 2016). Despite these findings, the topography of the relationship between imaging biomarkers as it pertains to nigrostriatal damage has not yet been described in detail.

In descriptive anatomy, neuronal tracing and staining studies define two cellular tiers of the SNc; a calbindin-positive dorsal tier which encompasses the ventral tegmental area and a calbindin-negative ventral tier, which spreads laterally toward the substantia nigra pars reticulata (SNr) (Lynd-Balta and Haber, 1994; Haber *et al.*, 2000; Haber, 2014). In Parkinson's disease, the pattern of nigral

neuronal loss differs to normal ageing, exhibiting an exponential decay with ~45% reduction over the first decade of illness, beginning and most prominently affecting the lateral ventral tier before spreading to the medial ventral and dorsal tiers. This is at variance to the linear fallout observed in healthy ageing that is estimated at 4.7–6% per decade and the relative sparing of the ventral compared to the dorsal tiers (Fearnley and Lees, 1991; Gibb and Lees, 1991). Meanwhile, the striatum is characterized by a rostrocaudal gradient of dopaminergic denervation with relative indemnity of caudate nucleus (Bernheimer *et al.*, 1973; Nyberg *et al.*, 1983; Kish *et al.*, 1988; Scherman *et al.*, 1989; Lee *et al.*, 2000; Cheng *et al.*, 2010; Oh *et al.*, 2012; Han *et al.*, 2016). This Parkinson's disease-related gradient is different to equivalent age-related declines of ~5–8% per decade across the putamen and caudate in healthy individuals (Ishibashi *et al.*, 2009; Shingai *et al.*, 2014). Evidence from animal work on nigrostriatal topography indicates that neurons originating in the SNc dorsal tier project predominantly to the head of the caudate and anterior putamen, while those of the ventral tier project to the posterior putamen and posterior caudate nuclei (Carpenter and Peter, 1972; Szabo, 1980; Lynd-Balta and Haber, 1994; Haber *et al.*, 2000; Haber, 2014).

In this context, the current exploratory multimodal imaging study uses neuromelanin-sensitive MRI and PET with ^{11}C -PE2I [a radioligand with high striatal binding (Jucaite *et al.*, 2006) and substantially greater DAT specificity than ^{123}I -FP-CIT or ^{123}I - β -CIT (Abi-Dargham *et al.*, 1996; Emond *et al.*, 1997; Guilloteau *et al.*, 1998) that is highly correlated with Parkinson's disease symptom severity (Li *et al.*, 2018)] to examine the association between deficits in neuromelanin content in the SNc and reductions in DAT density in a Parkinson's disease cohort with bilateral disease. Importantly, we take into account the distinct anatomical subregions of both the SNc and the striatum, the reported topography of their neuronal connections and the lateralization of clinical presentation, aiming to describe more comprehensively the association between the two imaging markers *in vivo* using an exploratory approach. While we expected there to be a relationship between neuromelanin and DAT density, based on available data, no specific hypotheses regarding its topography or extent were made.

Materials and methods

Subjects

Thirty non-demented mild-to-moderate stage Parkinson's disease patients and 15 healthy control subjects were recruited from specialist movement disorder clinics and local advertisement, respectively, under the TRANSEURO (<http://www.transeuro.org.uk/>) and PaMIR (Parkinson MRI Imaging Repository) research projects. Diagnosis of Parkinson's disease was performed by movement disorder specialists in accordance

with the Parkinson's UK Brain Bank Criteria (Hughes *et al.*, 1992), excluding atypical parkinsonism, concomitant vascular load, history of cognitive impairment, psychiatric disorders and factors that would preclude MRI scanning.

Patients were instructed to withdraw from all standard release anti-Parkinson's disease medications 24 h prior to motor and imaging assessments and 48 h for prolonged release medications. This included levodopa, dopamine agonists, catechol-O-methyltransferase and monoamine oxidase B inhibitors. Caffeine in any form was not permitted within 12 h prior to scan. Levodopa equivalent daily dosage (LEDD) for each participant was calculated (Tomlinson *et al.*, 2010).

The Movement Disorders Society Unified Parkinson's Disease Rating Scale Part-III (UPDRS-III) (Goetz *et al.*, 2008) administered by two experienced raters was used to calculate total motor severity in the practically defined OFF medicated state and subdivided into bradykinesia (items 4–8 and 14), rigidity (item 3), tremor (items 15–18) and axial (items 1–2 and 9–13) subscores. Clinical laterality was established based on clinical history recorded by the neurology unit at which patients were diagnosed. Asymmetry was also evaluated at research appointments during the study, derived from the sum of the UPDRS-III laterality items in the practically-defined OFF medicated state.

Ethical approval was obtained from the local Research Ethics Committees for TRANSEURO (IRAS: 57821, 65071, 78574; EPN2013/758, IK2013/685) and PaMIR (IRAS: 124223). Participant consent was obtained in writing in accordance with the Declaration of Helsinki.

Image acquisition

All scans were conducted at Invicro LLC (Hammersmith Hospital, London).

MRI

MRI scans were acquired for all Parkinson's disease and healthy control participants on a 3 T Siemens Magnetom Trio system with 32-channel head coil and consisted of neuromelanin-sensitive T₁-weighted TSE (repetition time = 829 ms; echo time = 12 ms; flip angle = 123°; echo train length = 4; echo spacing = 11.5 ms; low specific absorption rate; field of view = 256 × 256 mm; matrix size = 320 × 320) and high resolution volumetric T₁-weighted magnetization prepared rapid acquisition gradient echo (MPRAGE: repetition time = 2300 ms; echo time = 2.98 ms; flip angle = 9°; time to inversion = 900 ms; GRAPPA acceleration factor PE = 2; field of view = 240 × 256 mm; matrix size = 240 × 256) sequences.

For the MPRAGE, one whole brain volume was acquired consisting of 160 contiguous slices of 1 mm thickness. For the TSE, 12 slices of 2.5 mm thickness and slice gap of 0.25 mm were acquired parallel to the anterior-posterior commissure (AC-PC) line with coverage of the whole midbrain and upper pons. Scans lasted 301 and 332 s, respectively and patients were instructed to remain as still as possible for the duration.

PET

Parkinson's disease participants ($n = 30$) underwent ^{11}C -PE2I ([^{11}C]N-(3-iodopro-2E-enyl)-2 β -carbomethoxy-3 β -(4'-methylphenyl)nortropane) PET scans, acquired on a Siemens Biograph TruePoint HI-REZ 6 PET/CT system. Patients were

positioned supine such that the transaxial plane was parallel to the AC-PC plane and movement minimized using memory foam padding and video monitoring to aid repositioning. ^{11}C -PE2I tracer volumes were prepared to 10 ml using saline solution and administered intravenously as a single bolus injection followed immediately by 10 ml saline flush (injected dose = 325.85 ± 35.24 MBq; injected mass = 3.99 ± 1.89 μg). Administration was at a rate of 1 ml/s.

Dynamic emission data were acquired continuously while patients were at rest for 90 min post-injection. Data were binned into a dynamic series of 26 temporal frames (8×15 s, 3×60 s, 5×120 s, 5×300 s, 5×600 s) and reconstructed with corrections for decay, scatter and attenuation using a filtered back-projection algorithm (direct inversion Fourier transform) with a matrix size of 128×128 , zoom of 2.6 and 2 mm isotropic pixel size and smoothed using a 3D 5 mm full-width at half-maximum (FWHM) trans-axial Gaussian image filter. A low-dose CT transmission scan (0.36 mSv) was acquired for attenuation and scatter correction.

Image processing and region of interest analysis

Neuromelanin-sensitive MRI

For the quantitative evaluation of neuromelanin-sensitive MRI scans, study-specific templates were first created using grey and white matter MPRAGE segmentations from both Parkinson's disease and healthy control participants and diffeomorphic anatomical registration through exponentiated Lie algebra (DARTEL) in SPM12. Software defaults were modified to enable template and MPRAGE-to-template warp field generation in native voxel size (1 mm³). Neuromelanin-sensitive T₁-weighted images were co-registered to the corresponding MPRAGE and DARTEL warp fields applied in one step to normalize all images to common space. The neuromelanin template could then be generated through voxel-wise averaging (mean) over the entire cohort ($n = 45$).

Mesencephalic regions of interest for the left or right SNc were manually defined on five contiguous axial slices of the neuromelanin template on which the neuromelanin-related hyperintensity of the SNc was visible, at the level of the red nucleus and the inferior colliculus, in FSL (Jenkinson *et al.*, 2012). The volume of the SNc on each axial slice was divided into two sections representing the ventral (SNc^{ven}) and dorsal (SNc^{dor}) tiers, in accordance with post-mortem histological investigations on the spatial distribution of dopamine neurons relating to the striatal afferences of the SNc (Lynd-Balta and Haber, 1994; Haber *et al.*, 2000; Haber, 2014). The decussation of the superior cerebral peduncle (CP) was also defined on the same axial slices as a reference region (Fig. 1). Once all regions of interest were delineated the inverse DARTEL warp fields for each participant were applied to generate individualized regions of interest for sampling in native space. This was performed to reduce the effect of warping or normalization on the absolute voxel intensities within the images. Registration was checked visually in FSL before extracting mean region of interest intensity values using the `fsmeans` command. Neuromelanin contrast ratios were calculated in accordance with Sasaki and colleagues (2006) using the formula: $(\text{SNc} - \text{CP}) / \text{CP}$ for ventral and dorsal tiers separately. Contrast ratios were first calculated for the most and least

affected sides for each region of interest before averaging across sides to yield bilateral regional contrast ratios. Contrast ratios of the whole SNc i.e. SNc^{ven} and SNc^{dor} combined (SNc^{com}) were also calculated.

^{11}C -PE2I PET

Preprocessing and kinetic modelling for MPRAGE and ^{11}C -PE2I PET was conducted using MIAKATTM v3.4.2. (Molecular Imaging and Kinetic Analysis Toolbox, Imanova Imaging Centre, London, UK) (Gunn *et al.*, 2016), which uses FSL (FMRIB Image Analysis Group, Oxford, UK) (Jenkinson *et al.*, 2012), SPM (Statistical Parametric Mapping, Wellcome Trust Centre for Neuroimaging, London, UK) and in-house preprocessing and kinetic modelling procedures within an integrated PET analytical framework and is implemented in MATLAB[®] (Mathworks, Natick, MA, USA).

First, MPRAGE images were brain extracted, segmented and rigid-body registered to the Montreal Neurological Institute (MNI) template (Mazziotta *et al.*, 1995). MPRAGE images in 'pseudo-MNI' space (MPRAGE_{REG}) were then used for manual subcortical region of interest delineation in Analyze11.0. Afferent striatal dopaminergic connections from mesencephalic neurons show a distinctive dorsal-ventral pattern. The nigral dorsal tier projects to the ventromedial striatum while the ventral tier projects to the central associative and dorsal striatum (Lynd-Balta and Haber, 1994; Haber *et al.*, 2000; Haber, 2014). Striatal subdivision was conducted in accordance with the anatomical landmark-based methods derived from work on the *in vivo* distribution of D3 receptors using ^{11}C -(+)-PHNO (Tziortzi *et al.*, 2011). In brief, the putamen was subdivided into three sections on the axial plane; posterior to the AC (post-commissural putamen), anterior to the AC and dorsal to the posterior commissure (pre-commissural dorsal putamen), anterior to the AC and ventral to the posterior commissure (pre-commissural ventral putamen). The caudate was subdivided into two sections on the axial plane; anterior to the AC (pre-commissural caudate) and posterior to the AC (post-commissural caudate) (Fig. 1A and B). Regions of interest of the whole putamen and caudate nucleus were formed by merging pre-commissural and post-commissural subdivisions of the putamen and caudate, respectively. Furthermore, the striatum was defined as the combination of the putamen and caudate nucleus. Cerebellar grey matter was automatically defined by applying the deformation fields estimated from the spatial normalization (12-parameter affine transformation followed by non-linear warp) of the MNI template to the MPRAGE_{REG}, to an MNI-based regional atlas (CIC Atlas v1.2.). Grey matter segmentation maps were then applied to isolate cerebellar grey matter. Regions of interest for the SNc^{ven} and SNc^{dor}, which were defined on the study-specific template as described in the previous section, were also brought into MPRAGE_{REG} space by applying the inverse DARTEL warp fields and rigid body registration parameters (native-to-pseudo-MNI) in one step.

Motion correction was conducted on the dynamic PET data to correct for intra-scan head movement using frame-to-frame rigid registration with the 16th frame (corresponding to 780–900 s post-injection) as a reference, chosen because of high signal-to-noise ratio. No image artefacts due to substantial head movement were observed for any of the patients included in this study. Realigned frames corresponding to 10–90 min

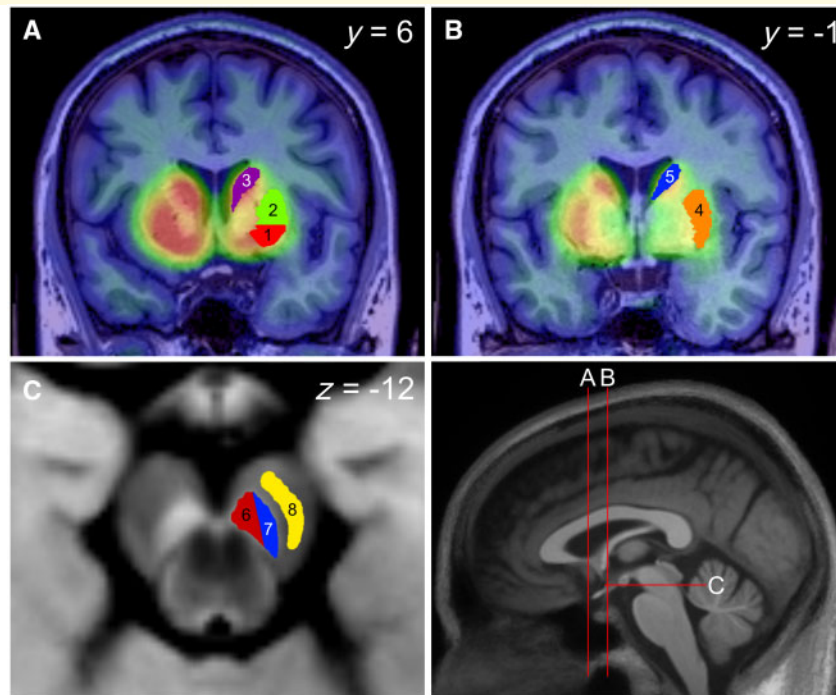


Figure 1 Region of interest definition in the substantia nigra and striatum. *Bottom right:* Sagittal midline view of a 3D T_1 -weighted MPRAGE template, derived using DARTTEL with 30 Parkinson's disease and 15 healthy control participants. The red line annotations illustrate the position of the coronal and axial planes corresponding to the sections depicted in **A–C**. (**A** and **B**) ^{11}C -PE2I ADD images overlaid onto the structural MPRAGE_{REG} from two levels of the coronal plane either side of the anterior commissure along the y -axis. Regions of the pre-commissural striatum (**A**) consist of ventral putamen (1, red), dorsal putamen (2, green) and caudate (3, purple). Regions of the post-commissural striatum (**B**) include putamen (4, orange) and caudate (5, blue). (**C**) An axial slice of the neuromelanin-sensitive T_1 -weighted template derived using DARTTEL ($n = 45$) at the level of the SNc, including delineation of the dorsal (6, red) (SNc^{dor}) and ventral (7, blue) (SNc^{ven}) tiers, as well as cerebral peduncle (8, yellow). Descriptive anatomy demonstrates projections from the dorsal tier (6, red) to striatal regions 1–3 while the ventral tier (7, blue) projects to regions 2–5 (Lynd-Balta and Haber, 1994; Haber *et al.*, 2000; Haber, 2014).

were subsequently summed to obtain signal-averaged (ADD) images that were then co-registered to the subjects MPRAGE_{REG} using normalized mutual information as the cost function. The derived registration parameters were applied to bring the dynamic PET data into alignment with the MPRAGE_{REG} and corresponding region of interest map. PET image processing was evaluated at each step before region of interest maps were applied to the dynamic PET frames to generate regional time-activity curves (TACs) for all regions of interest on the most and least affected sides separately as well as bilaterally. The simplified reference tissue model (SRTM) (Lammertsma and Hume, 1996) was used to calculate regional non-displaceable binding potential (BP_{ND}). Cerebellar grey matter was used as a reference as previous studies have demonstrated negligible tracer uptake in this region (Hall *et al.*, 1999; Halldin *et al.*, 2003; Jucaite *et al.*, 2006).

Registered frames between 10–90 min were subsequently summed to obtain ADD images that were co-registered to the subjects MPRAGE_{REG} using normalized mutual information as a cost function. Approximated co-registration matrices were then applied to both ADD images and realigned dynamic frames so that all images were in register with the subject MPRAGE_{REG} and the corresponding region of interest map.

Statistical analysis

All statistical analyses were performed using R version 3.4.3 (R Core Team, 2017) and packages 'afex' (Singmann *et al.*, 2017), 'emmeans' (Lenth, 2018) and 'Hmisc' (Harrell Jr, 2017).

Demographic data were compared between Parkinson's disease and healthy control groups using independent t -tests and Fisher's exact test. To assess differences in neuromelanin contrast ratios between groups and regions of the SNc, a mixed ANOVA was conducted with group (Parkinson's disease, healthy control) as the between-subjects factor and region (bilateral SNc^{ven}, bilateral SNc^{dor}) as the within-subjects factor.

To assess lateralization of SNc neuromelanin content, contrast ratio asymmetry indices (Seibyl *et al.*, 1995) were calculated for the SNc^{ven} and SNc^{dor} according to clinical laterality in the Parkinson's disease group (most/least affected) and right/left in the healthy control group and compared using one-tailed independent t -tests. Within the Parkinson's disease group, lateralization was assessed for both SNc neuromelanin content and DAT density using two-way repeated measures ANOVA, with neuromelanin contrast ratio or ^{11}C -PE2I BP_{ND} as the dependent variable and region (SNc^{ven}, SNc^{dor}) and side (most/least affected) as within-subjects factors.

Linear relationships between neuromelanin contrast ratios in the SNc and ^{11}C -PE2I BP_{ND} values in the striatum were tested using simple linear regression. Not all regional combinations between SNc and striatum were assessed; instead, planned tests were performed based on previous anatomical work mapping connectivity between subregions of the substantia nigra and striatum (Lynd-Balta and Haber, 1994; Haber *et al.*, 2000; Haber, 2014). As such, regression analyses were conducted between neuromelanin contrast ratio (independent variable) in the SNc^{ven} [Fig. 1C(7)] and ^{11}C -PE2I BP_{ND} (dependent variable) in the pre-commissural dorsal putamen and caudate [Fig. 1A(2–3)] as well as the post-commissural putamen and caudate [Fig. 1B(4–5)]; and between neuromelanin contrast ratio in the SNc^{dor} [Fig. 1C(6)] and ^{11}C -PE2I BP_{ND} in the pre-commissural ventral putamen, dorsal putamen and caudate [Fig. 1A(1–3)]. Regression analyses were also conducted between neuromelanin contrast ratio and ^{11}C -PE2I BP_{ND} values within the SNc^{ven} and SNc^{dor}. Analyses were performed for the most and least affected sides separately.

Pearson's product moment correlation coefficient (one-tailed) was used to explore relationships between each measure of disease severity (disease duration, UPDRS-III subscores; bradykinesia, rigidity, tremor, axial) and neuromelanin contrast ratios for bilateral nigral regions (SNc^{ven}, SNc^{dor}) as well as ^{11}C -PE2I BP_{ND} for bilateral nigral and striatal subregions (SNc^{ven}, SNc^{dor}, pre-commissural dorsal putamen, pre-commissural ventral putamen, pre-commissural caudate, post-commissural putamen and post-commissural caudate).

The Benjamini-Hochberg procedure was used to control the false discovery rate (FDR) across all planned correlation and regression analyses simultaneously, at a desired threshold of $P < 0.05$.

Normal distribution was assessed graphically using normal probability plots as appropriate, extreme values were evaluated using Z-scores, boxplots and studentized residuals, independence of observations using Durbin-Watson statistic and homoscedasticity assessed by residual plots and Levene's test.

Data availability

The authors confirm that data presented in this article are original. The data that support the findings of this study are available from the corresponding author, upon reasonable request.

Results

Demographics

Clinical and demographic characteristics for the Parkinson's disease and healthy control groups are summarized in Table 1. There were no significant differences in age or gender between groups.

Neuromelanin in the substantia nigra in Parkinson's disease compared to healthy controls

Mixed ANOVA showed a main effect of group [$F(1,43) = 11.95$, $P = 0.001$], in which neuromelanin

contrast ratios were significantly lower in Parkinson's disease [mean_{EM} = 0.095, 95% confidence interval (CI) (0.081, 0.109)] as compared to the healthy controls [mean_{EM} = 0.129, 95% CI (0.115, 0.143)]. There was also a main effect of region [$F(1,43) = 41.35$, $P < 0.001$] whereby SNc^{ven} [mean_{EM} = 0.100, 95% CI (0.090, 0.110)] showed significantly lower neuromelanin contrast ratios than SNc^{dor} [mean_{EM} = 0.124, 95% CI (0.114, 0.134)]. However, no significant group \times region interaction was detected [$F(1,43) = 0.71$, $P = 0.404$] (Fig. 2). Including age and gender as covariates did not alter results.

Lateralization of neuromelanin and dopamine transporters in Parkinson's disease

Asymmetry indices showed no significant differences between Parkinson's disease and healthy control groups for SNc^{ven} [$t(43) = 0.75$, $P = 0.230$] or SNc^{dor} [$t(43) = 1.42$, $P = 0.081$]. Removal of one extreme outlier (Table 2) did not alter results.

Two-way repeated measures ANOVA conducted on the Parkinson's disease group revealed no significant interaction between region (SNc^{ven}, SNc^{dor}) and side (most/least affected) on either neuromelanin contrast ratio [$F(1,29) = 0.17$, $P = 0.685$] (Fig. 3A) or ^{11}C -PE2I BP_{ND} [$F(1,29) = 0.34$, $P = 0.563$] (Fig. 3B). However, for neuromelanin contrast ratio, there was a marginally significant main effect of side [$F(1,29) = 4.85$, $P = 0.036$], whereby neuromelanin contrast ratio was lower in the most affected hemisphere [mean = 0.097, 95% CI (0.084, 0.109)] than in the least affected hemisphere [mean = 0.104, 95% CI (0.092, 0.117)], and a main effect of region [$F(1,29) = 36.19$, $P < 0.001$] in which SNc^{ven} [mean = 0.087, 95% CI (0.074, 0.100)] was significantly lower than SNc^{dor} [mean = 0.114, 95% CI (0.101, 0.127)]. Similarly for ^{11}C -PE2I BP_{ND}, there was a marginally significant main effect of side [$F(1,29) = 4.21$, $P = 0.049$], in which ^{11}C -PE2I BP_{ND} was lower in the most affected hemisphere [mean = 0.633, 95% CI (0.584, 0.684)] than in the least affected hemisphere [mean = 0.667, 95% CI (0.618, 0.717)], and a main effect of region [$F(1,29) = 76.39$, $P < 0.001$], whereby SNc^{ven} [mean = 0.607, 95% CI (0.558, 0.655)] was significantly lower than SNc^{dor} [mean = 0.694, 95% CI (0.646, 0.743)]. Including age and gender as covariates did not alter results.

In terms of percentage of regional neuromelanin contrast ratio reduction, the Parkinson's disease group showed a ventro-dorsal pattern of neurodegeneration as compared to healthy controls as follows SNc^{ven} (−30.03%) > SNc^{dor} (−21.45%) (Table 2).

Relationship between neuromelanin and DAT density in the nigrostriatal system

On the most affected side, significant positive relationships were found between neuromelanin contrast ratio

Table 1 Demographic and clinical characteristics of Parkinson's disease and healthy control groups

	Parkinson's disease	Healthy controls	Statistic	P
Gender, male:female ^a	26:4	9:6	–	0.062
Age, years ^b	55.58 ± 6.69	56.96 ± 10.43	$t(19.96) = 0.47$	0.646
Disease duration, years	6.78 ± 1.88 [4.09–10.14]	–	–	–
UPDRS-III total	34.93 ± 10.64 [16–53]	–	–	–
UPDRS-III bradykinesia	15.03 ± 5.44 [3–26]	–	–	–
UPDRS-III rigidity	7.23 ± 3.13 [3–14]	–	–	–
UPDRS-III tremor	8.33 ± 5.59 [0–19]	–	–	–
UPDRS-III axial	4.33 ± 2.11 [1–12]	–	–	–
Hoehn and Yahr scale	2.00 ± 0.00	–	–	–
LEDD	766.73 ± 359.47	–	–	–

Values represent the mean ± standard deviation. Range is reported in square brackets for disease duration and UPDRS-III scores. The UPDRS-III was administered while patients were in the practically-defined OFF medicated state; 24 h for standard release and 48 h for prolonged release medications. Subscale range (min–max) for bradykinesia (0–44), rigidity (0–20), tremor (0–40) and axial (0–28). LEDD = levodopa equivalent daily dose.

^aSignificant differences were tested using Fisher's Exact test.

^bSignificant differences were tested using independent t-tests.

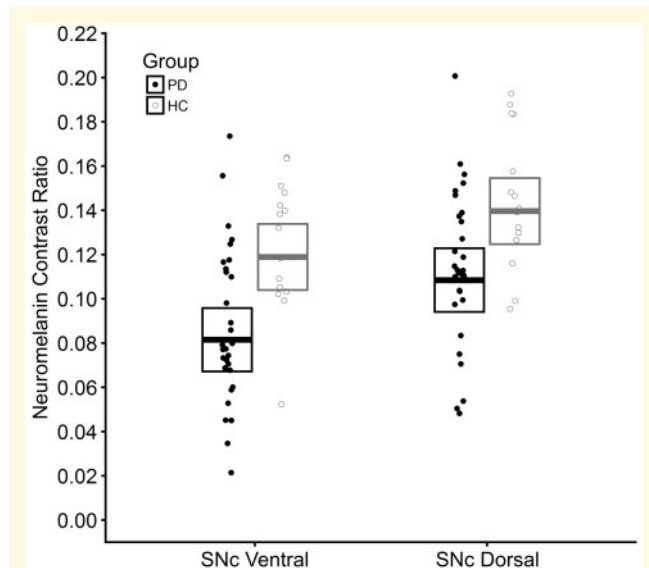


Figure 2 Neuromelanin loss in the ventral and dorsal tiers of the substantia nigra pars compacta in Parkinson's disease as compared to healthy controls. Strip plot illustrating neuromelanin contrast ratio values for individuals of both Parkinson's disease (PD) and healthy control (HC) groups and for each subregion of the SNc (ventral tier, dorsal tier). Filled circles represent individuals within the Parkinson's disease group and open grey circles represent individuals within the healthy control group. Crossbars represent 95% confidence intervals about the estimated marginal mean derived from the mixed ANOVA analysis.

in the SNc^{ven} and ¹¹C-PE2I BP_{ND} in the pre-commissural dorsal putamen [$F(1,28) = 13.82$, $P = 0.001$] and caudate [$F(1,28) = 15.13$, $P = 0.001$] and the post-commissural putamen [$F(1,28) = 13.05$, $P = 0.001$] (Fig. 4). Neuromelanin contrast ratio in the SNc^{dor} was positively associated with ¹¹C-PE2I BP_{ND} in the pre-commissural dorsal putamen [$F(1,28) = 7.99$, $P = 0.009$], and caudate

[$F(1,28) = 23.12$, $P < 0.001$] (Fig. 5). Trends were found between neuromelanin contrast ratio in the SNc^{ven} and ¹¹C-PE2I BP_{ND} in the post-commissural caudate [$F(1,28) = 5.13$, $P = 0.031$] and between neuromelanin contrast ratio in the SNc^{dor} and ¹¹C-PE2I BP_{ND} in the pre-commissural ventral putamen [$F(1,28) = 5.22$, $P = 0.030$]; however, after Benjamini-Hochberg FDR correction across all correlational tests, these results did not remain significant. Inclusion of additional covariates age and gender in the above regression models had only minimal impact upon the beta coefficients associated with the main independent variable (difference of $3.96 \pm 2.92\%$) and did not result in changes to significance level. No significant relationship was found between neuromelanin contrast ratio and ¹¹C-PE2I BP_{ND} within either SNc^{ven} or SNc^{dor} (Figs 4 and 5).

On the clinically least affected side, there were no significant relationships between neuromelanin contrast ratio and ¹¹C-PE2I BP_{ND} within the ventral or dorsal SNc or with ¹¹C-PE2I BP_{ND} in striatal subregions (Figs 4 and 5).

Relationship between clinical severity and neuromelanin and DAT density

SNc neuromelanin contrast ratio was inversely related to disease duration, particularly within the ventral tier, while no association with UPDRS-III bradykinesia, rigidity or axial subscales was evident. In contrast, SNc ¹¹C-PE2I BP_{ND} appeared to show an opposing pattern whereby negative correlations were evident with UPDRS-III bradykinesia, rigidity or axial subscales but not disease duration. In the striatum, ¹¹C-PE2I BP_{ND} appeared to correlate relatively consistently with disease duration and UPDRS-III bradykinesia, rigidity and axial subscales. No significant correlations were found between UPDRS-III tremor and any imaging measure (Fig. 6).

Table 2 Mean neuromelanin contrast ratios, ^{11}C -PE2I BP_{ND} values, per cent decline and asymmetry indices

	Healthy control (n = 15)		Parkinson's disease (n = 30)						
	Bilateral	AI	MA	%	LA	%	Bilateral	%	AI ^a
Neuromelanin contrast ratio									
SNC combined (SNC ^{com})	0.14 ± 0.03	-0.17 ± 18.98	0.10 ± 0.03	71.79	0.11 ± 0.04	77.99	0.10 ± 0.03	74.89	6.25 ± 19.30
Ventral tier (SNC ^{ven})	0.12 ± 0.03	2.24 ± 26.23	0.08 ± 0.04	66.62	0.09 ± 0.04	73.32	0.09 ± 0.04	69.97	5.54 ± 32.23
Dorsal tier (SNC ^{dor})	0.15 ± 0.03	-3.07 ± 20.44	0.11 ± 0.03	76.31	0.12 ± 0.04	80.79	0.11 ± 0.03	78.55	4.43 ± 17.99
^{11}C-PE2I BP_{ND}									
SNC combined (SNC ^{com})	–	–	0.63 ± 0.13	–	0.67 ± 0.14	–	0.65 ± 0.13	–	5.76 ± 14.50
Ventral tier (SNC ^{ven})	–	–	0.59 ± 0.11	–	0.62 ± 0.14	–	0.61 ± 0.12	–	3.97 ± 18.54
Dorsal tier (SNC ^{dor})	–	–	0.67 ± 0.15	–	0.71 ± 0.16	–	0.69 ± 0.14	–	5.67 ± 16.57
Striatum	–	–	1.68 ± 0.49	–	2.03 ± 0.61	–	1.85 ± 0.52	–	20.20 ± 16.49
Putamen	–	–	1.17 ± 0.37	–	1.53 ± 0.53	–	1.35 ± 0.41	–	27.06 ± 21.79
Pre-commissural dorsal putamen	–	–	1.04 ± 0.45	–	1.46 ± 0.66	–	1.23 ± 0.49	–	35.22 ± 29.71
Pre-commissural ventral putamen	–	–	1.94 ± 0.64	–	2.47 ± 0.83	–	2.19 ± 0.67	–	25.45 ± 22.47
Post-commissural putamen	–	–	0.70 ± 0.16	–	0.94 ± 0.36	–	0.82 ± 0.25	–	26.71 ± 21.97
Caudate	–	–	2.00 ± 0.68	–	2.37 ± 0.76	–	2.18 ± 0.69	–	19.71 ± 17.33
Pre-commissural caudate	–	–	2.21 ± 0.78	–	2.60 ± 0.87	–	2.39 ± 0.79	–	19.29 ± 18.08
Post-commissural caudate	–	–	1.18 ± 0.41	–	1.47 ± 0.49	–	1.32 ± 0.43	–	23.88 ± 23.05

Mean (\pm SD) neuromelanin contrast ratios in the SNc are shown for both the Parkinson's disease and healthy control groups bilaterally and for the clinically most and least affected sides for the Parkinson's disease group. Change in neuromelanin contrast ratios for the Parkinson's disease group is expressed as a percentage relative to the healthy control group. Mean (\pm SD) asymmetry indices (AI) for both the Parkinson's disease (most/least affected) and healthy control groups (right/left) and mean (\pm SD) ^{11}C -PE2I BP_{ND} values in the SNc and striatum for the Parkinson's disease group are also shown.

^aRemoval of one outlier for asymmetry indices > 3 SD away from the mean.

AI = asymmetry index; BP_{ND} = non-displaceable binding potential; LA = least affected; MA = most affected.

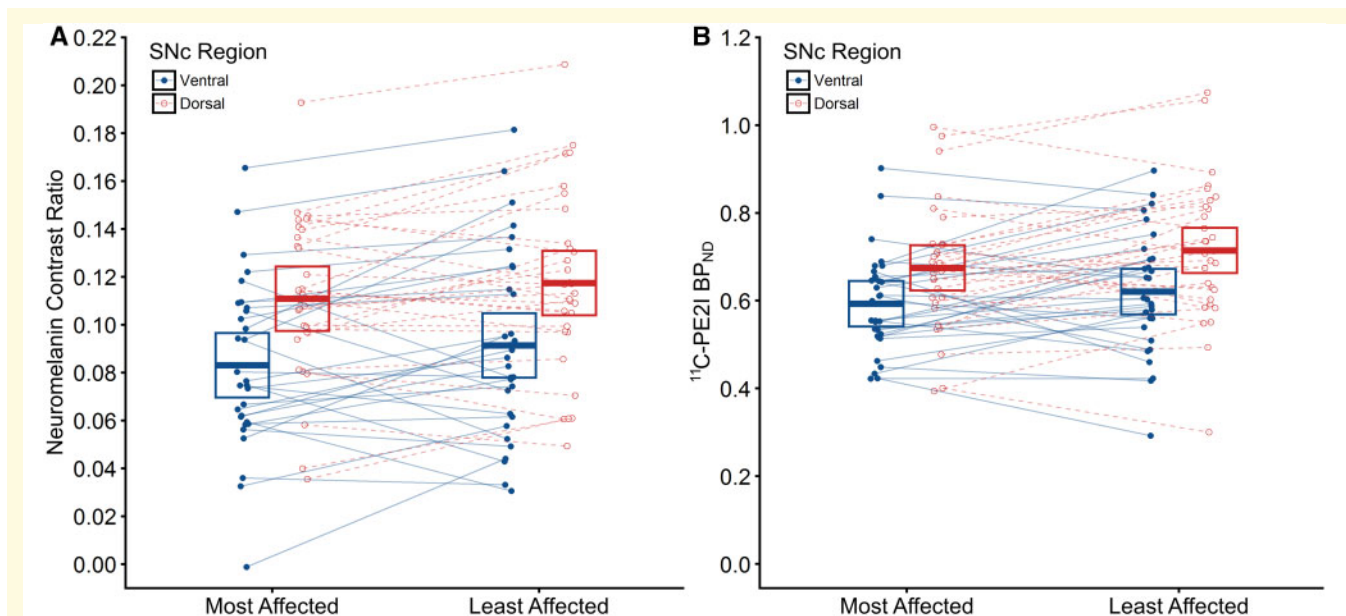


Figure 3 Lateralization of neuromelanin loss and DAT density in the ventral and dorsal tiers of the substantia nigra pars compacta for the clinically-defined most and least affected sides. Strip plots showing neuromelanin contrast ratio (A) and ^{11}C -PE2I BP_{ND} (B) values for individuals within the Parkinson's disease group as a function of the clinically-defined most/least affected side and subregion of the SNc (ventral tier, dorsal tier). Filled blue circles represent the ventral tier while open red circles represent the dorsal tier. Points between the clinically-defined most and least affected sides are connected with either a solid blue line (ventral tier) or a dashed red line (dorsal tier) to illustrate asymmetry within individuals. Crossbars represent 95% confidence intervals about the mean.

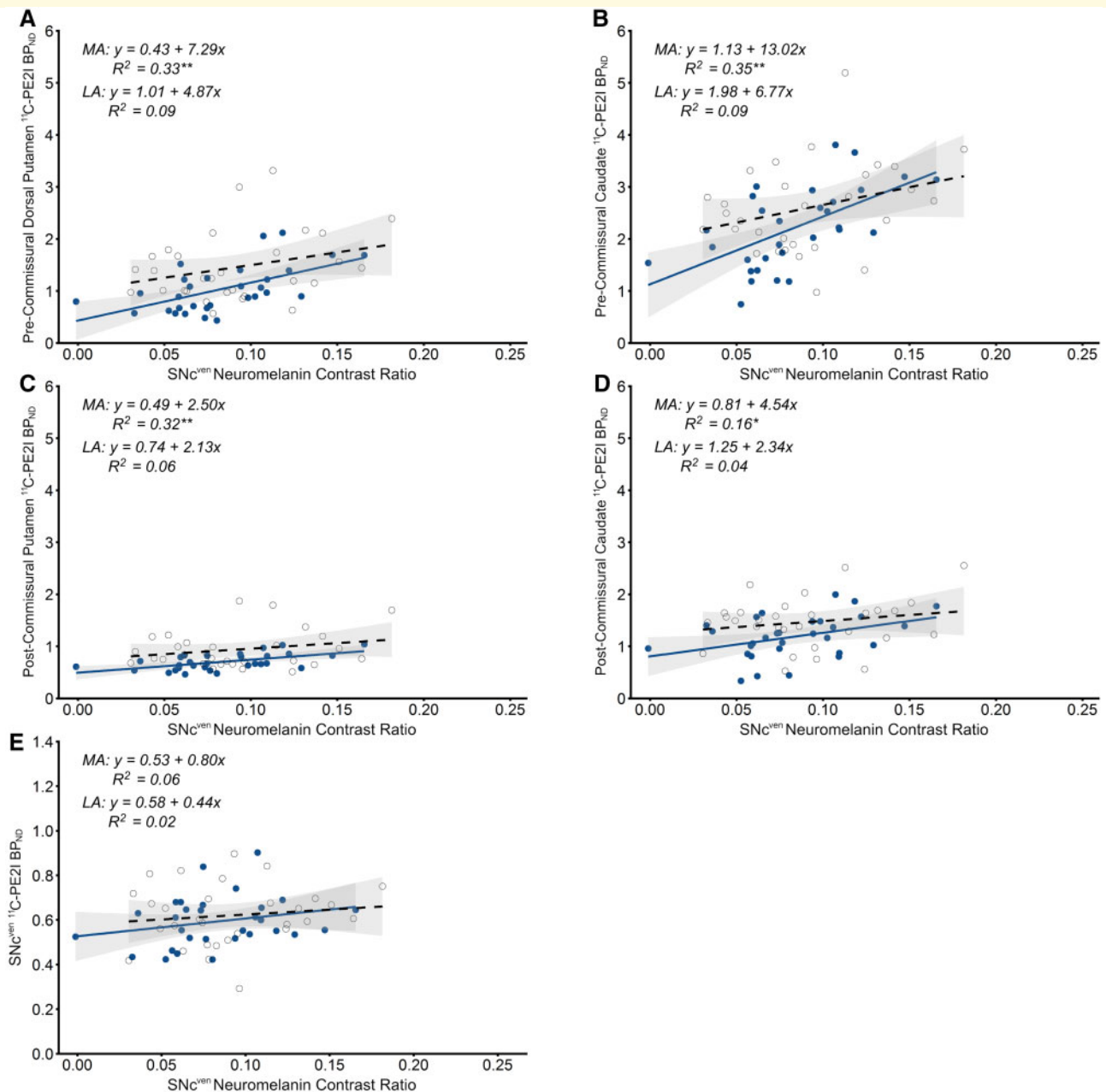


Figure 4 Association between neuromelanin in the substantia nigra pars compacta ventral tier and nigrostriatal dopamine transporter binding. Scatterplots and simple linear regression showing positive relationships between neuromelanin contrast ratio in the SNc^{ven} and $^{11}\text{C-PE2I BP}_{\text{ND}}$ in the pre-commissural dorsal putamen (**A**), pre-commissural caudate (**B**), post-commissural putamen (**C**), post-commissural caudate (**D**) and SNc^{ven} (**E**) in the clinically-defined most affected (filled blue circles, solid line) and least affected sides (open circles, dashed line). Grey shaded areas represent 95% confidence intervals. ******Significant result following Benjamini-Hochberg FDR correction for all correlational tests. *****Significance at $P < 0.05$. BP_{ND} = non-displaceable binding potential; LA = least affected; MA = most affected.

Discussion

Neuromelanin loss in the substantia nigra

The present study assessed the integrity of nigrostriatal pathways *in vivo* in a moderate stage Parkinson's disease

cohort by using neuromelanin-sensitive MRI and $^{11}\text{C-PE2I}$ PET. As expected, Parkinson's disease subjects had reduced neuromelanin when compared to controls, in line with previous investigations. While Sasaki *et al.* (2006) in their seminal paper examining neuromelanin *in vivo* report contrast ratio values almost double to what is reported here, our data show a larger effect size in equivalent tests ($d = 1.1$

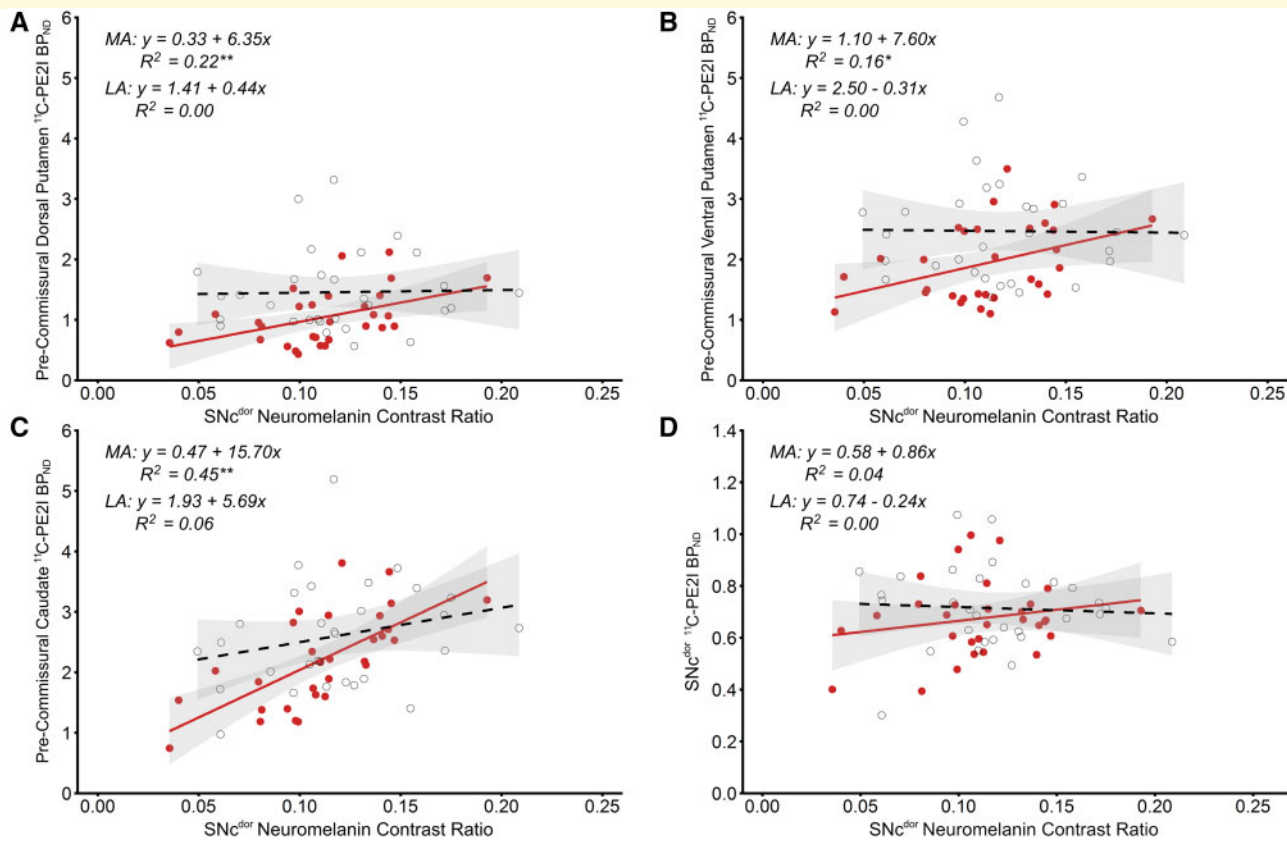


Figure 5 Association between neuromelanin in the substantia nigra pars compacta dorsal tier and nigrostriatal dopamine transporter binding. Scatterplots and simple linear regression showing positive relationships between neuromelanin contrast ratio in the SNc^{dor} and ¹¹C-PE2I BP_{ND} in the pre-commissural dorsal putamen (A), pre-commissural ventral putamen (B), pre-commissural caudate (C) and SNc^{dor} (D) in the clinically-defined most affected (filled red circles, solid line) and least affected sides (open circles, dashed line). Grey shaded areas represent 95% confidence intervals. ^{**}Significant result following Benjamini-Hochberg FDR correction for all correlational tests. ^{*}Significance at $P < 0.05$. BP_{ND} = non-displaceable binding potential; LA = least affected; MA = most affected.

and 0.8), with both studies having similar sensitivity to detect $d > 0.8$ with 80% power at α of 0.05. The disparity could be due to disease severity with the current cohort at 6.8 years of illness as compared to 2.5 years, or to the size and placement of regions of interest. The size of the circular cursors used for sampling by Sasaki *et al.* (2006) was not detailed, though they state that pixels in the high signal intensity areas were measured. In contrast, the semi-automated sampling method used here was not as influenced by the local hyperintensity in individual subjects. In addition, our cohort was ~ 15 years younger.

Relationship between nigral neuromelanin and striatal dopamine transporters

Our findings demonstrate that the relationship between nigral neuromelanin and striatal DAT in Parkinson's disease exhibits a remarkably lateralized pattern between the most and least affected brain hemispheres. Moderate to strong linear associations between the two measures were

detected across the two regions but only in the most affected side. It is possible this lateralization could be explained by ceiling effects and/or hemispheric lagging akin to that which has been observed in Parkinson's disease with striatal dopaminergic markers such as aromatic L-amino acid decarboxylase, vesicular monoamine transporter (type 2) and dopamine transporter (Lee *et al.*, 2000; Nandhagopal *et al.*, 2009). However, this alone seems unlikely given that significant depigmentation was found in both sides of the nigra, indicating that the neurodegenerative process in the least affected hemisphere had already begun in our cohort. If we assume that the neurodegenerative process occurs in a similar manner for both hemispheres, we might expect some degree of correlation between the two imaging measures on the least affected side, especially between regions with substantial SNc cell and striatal DAT loss. That this was not the case may be strong evidence to the contrary.

Alternatively, these measures might reflect different aspects of disease progression. In a comprehensive post-mortem investigation, Kordower *et al.* (2013) observed that loss of melanin-containing neurons in the SNc was

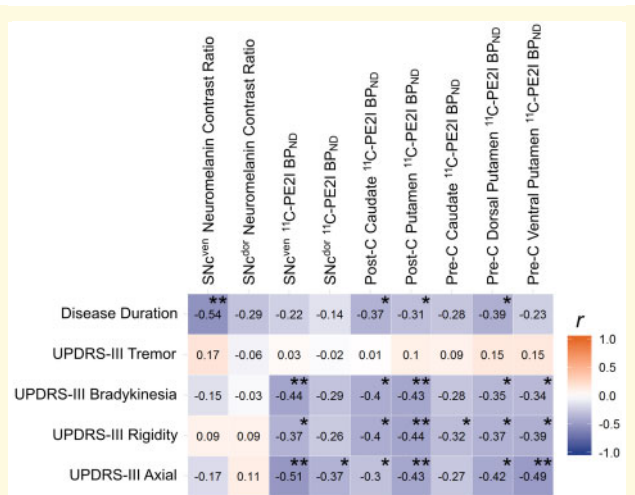


Figure 6 Relationship between measures of clinical severity and regional neuromelanin and dopamine transporter binding. Pearson's correlation matrix with measures of clinical severity by row and neuromelanin contrast ratio in the SNc and ¹¹C-PE2I BP_{ND} in the SNc and striatum by column. Tiles are colour coded and labelled with the value of the correlation coefficient. **Significant result following Benjamini-Hochberg FDR correction for all correlational tests. *Significance at $P < 0.05$. BP_{ND} = non-displaceable binding potential; Post-C = post-commissural; Pre-C = pre-commissural.

consistently outweighed by loss of tyrosine hydroxylase-positive neurons in the first two decades of illness. Thus, while DAT imaging may yield markers reflecting dopaminergic phenotype and neuronal dysfunction, neuromelanin markers may relate more closely to structure and neurodegeneration. It is possible this may explain why here, DAT tended to correlate with bradykinetic/rigid/axial severity while nigral neuromelanin correlated with disease duration, particularly within the nigra. Interestingly, these differential trajectories appear to converge and become less variable over time (Kordower *et al.*, 2013). It is feasible that this could account for the lateralization demonstrated here, where associations become apparent only when the extent of nigral neuromelanin loss comes in line with that of tyrosine hydroxylase-positive cell density.

Relationship between neuromelanin and dopamine transporters within the substantia nigra

In line with evidence from post-mortem data, Parkinson's disease subjects displayed a ventral to dorsal pattern of nigral depigmentation (Fearnley and Lees, 1991; Gibb and Lees, 1991; Kordower *et al.*, 2013) and showed a tendency for greater loss in the clinically-defined most affected side. Despite DAT density following a similar pattern of distribution, we did not observe any relationship between the two imaging markers. Similar results have also been

shown in a small cohort of young healthy males (Ito *et al.*, 2017). Recent nuclear imaging studies using ¹¹C-FeCIT and ¹⁸F-FE-PE2I PET in early and *de novo* patients have shown that the loss of DAT in the striatum (−35 to 70%) exceeds the loss in the substantia nigra (−25 to 30%), as compared to healthy controls (Caminiti *et al.*, 2017; Fazio *et al.*, 2018). One explanation for this relates to evidence suggesting that distal axonal degeneration occurs initially before proceeding retrograde towards the cell body (Calo *et al.*, 2016; Kurowska *et al.*, 2016; Tagliaferro and Burke, 2016). If this is the case then the relatively modest DAT loss in the nigra may represent delayed, slower or variable progression rate to that in the striatum. While this is yet to be studied, it could explain why the relationship with DAT differs between the nigra and striatum.

Comparison with previous studies

A few studies (Colloby *et al.*, 2012; Kraemmer *et al.*, 2014; Saari *et al.*, 2017) have evaluated the relationship between nigral neuromelanin and striatal DAT, using ante-mortem DAT-specific SPECT (¹²³I-FP-CIT or ¹²³I-β-CIT) with either post-mortem histochemistry of the SNc (conducted ~2.5–5 years after SPECT assessment) or neuromelanin-sensitive MRI. Positive correlations have been noted in mixed dementia cohorts (Colloby *et al.*, 2012) and in general neurological samples (Kraemmer *et al.*, 2014; Kuya *et al.*, 2016) and were in line with those found in smaller Parkinson's disease samples (Isaias *et al.*, 2016) and in the current Parkinson's disease-only cohort.

In contrast, Saari and colleagues (2017) found no significant correlations between nigral neuromelanin and striatal DAT in a small group of 11 Parkinson's disease and seven individuals with mixed parkinsonism. This may have been due to lack of power and/or inclusion of mixed parkinsonism, as correlation coefficients appear to graduate from zero/weak to moderate upon removal of non-Parkinson's disease patients from the analysis. The authors suggested that the relationship between nigral neuromelanin cell density and striatal DAT may dissipate as the disease progresses. Indeed, while results showing that nigral neuronal density in a mixed dementia cohort accounts for 58%, 40% and 20% of the variance in posterior and anterior putamen and caudate DAT, respectively, they appear to be driven mostly by non-Parkinson's disease individuals (Colloby *et al.*, 2012), with the Parkinson's disease dementia data tending towards an asymptote. In the current Parkinson's disease cohort, although significant relationships were found between both tiers of the nigra and their striatal afferents in the most affected side, it appeared that this association was strongest between the dorsal tier and pre-commissural caudate, which retains the highest DAT expression across the striatum (Nandhagopal *et al.*, 2009; Oh *et al.*, 2012; Han *et al.*, 2016). However, normative data from a group of healthy young males show that nigral neuromelanin accumulation does not correlate

with nigral DAT at baseline (Ito *et al.*, 2017). In addition, preclinical work demonstrates correlations in more pathologically advanced 6-OHDA mouse models but not in mild MPTP regimes (Alvarez-Fischer *et al.*, 2007). Thus, it is possible that the relationship between nigral neuromelanin content and striatal DAT is constrained by both ceiling and floor effects and may be evident only at some stages of Parkinson's disease progression.

Isaias and colleagues (2016) found no relationship between neuromelanin and DAT asymmetries, performing analyses on the whole nigra, putamen and caudate. Moreover, correlational analyses of absolute values involved collapsing across the most/least affected sides. Others have found positive results but using asymmetry indices calculated between left and right hemispheres (Kraemmer *et al.*, 2014; Kuya *et al.*, 2016), thus limiting pathological relevance and interpretability. The only study to perform correlations separately for most/least affected sides showed significant associations between asymmetry indices but no correlations of absolute values (Saari *et al.*, 2017). Importantly, however, these authors distinguished most/least affected sides as those with higher/lower cell count and/or DAT density. In the present study, while we found greater demelanization in the clinically most affected side we also noted that a significant proportion of our patients (~38%) displayed the opposite i.e. greater neuromelanin loss in the clinically least affected side, which was discordant to the side with greatest DAT loss. This finding has been discussed recently (Isaias *et al.*, 2016) and possibly stands as an important methodological factor to explain the discordance between results.

Limitations and considerations

There are some limitations in the current report. Delineation of the SNc was based on the hyperintense area of the midbrain on neuromelanin magnetic resonance images as it is not easily visible on standard structural scans, which could introduce bias towards overall greater values. We attempted to resolve this by using an automated procedure in which the SNc was delineated on neuromelanin templates created via normalization of structural scans from both Parkinson's disease and healthy control groups. In doing so, we were able to remain objective and consistent across individuals. Moreover, our data correspond well with percentage losses in a less advanced subset of nine patients (1–14 year disease duration, mean = 8 years) from Kordower and colleagues (2013), whose values indicate ~22% loss in the dorsal and ~35% in the ventral tiers. Second, while striatal regions of interest were defined according to anatomical landmark-based guidelines derived from a recent study on *in vivo* distribution of D3 receptors, parcellation could potentially be improved using connectivity-based methods such as probabilistic tractography (Chowdhury *et al.*, 2013). Age and gender have recently been shown to have significant effects over neuromelanin levels in

healthy individuals (Xing *et al.*, 2018). While we attempted to account for this through addition of covariates in our analyses, this constitutes incomplete control and thus the influence of these variables should be considered here and in future work. In addition, although striatal DAT in Parkinson's disease is well characterized using mostly SPECT ligands such as ¹²³I-FP-CIT, we did not obtain ¹¹C-PE2I scans for healthy controls. This would have enabled parallel analysis from which we could ascertain the normative nigrostriatal state across both brain hemispheres using the two imaging markers. Lastly, it has been shown that chronic exposure to dopaminergic drugs including levodopa and dopamine agonists can downregulate striatal DAT to varying degrees (–4 to 7.2%), depending on the exposure dose (Guttman *et al.*, 2001; Fahn *et al.*, 2004). As such, chronic exposure should be considered as a confounding factor in the current study.

Conclusions

The current study provides important insights into the relationship between neuromelanin content in the SNc and striatal DAT density in moderate stage Parkinson's disease, as measured *in vivo* using neuromelanin-sensitive MRI and ¹¹C-PE2I PET. Reduction of nigral pigmentation in Parkinson's disease displays an uneven pattern of association with the loss of striatal dopaminergic function towards the clinically most affected side while no relationship was found with nigral DAT. These findings may be indicative of a lag in disease progression or differences in the pathological processes measured that could manifest with heterogeneous rate of decline, convergence and symmetry. However, further work including longitudinal imaging assessment on the demelanization trajectories in the nigra, in both tiers and on the most and least affected side would provide a strong basis from which we could start to understand the relationship between these pathological processes.

Acknowledgements

We would like to thank Miss Natalie Valle-Guzman (University of Cambridge, UK), Prof. Tom Foltynie, Dr Zinovia Kefalopoulou, Dr Philipp Mahlknecht, Dr Viswas Dayal, Dr Dilan Athauda (University College London, UK), Prof. Håkan Widner, Assoc. Prof. Gesine Paul-Visse (Lund University, Sweden), Dr Alistair Church (Cardiff University, UK) and Dr Clare Loane (Imperial College London, UK) for their part in clinical management and co-ordination of neuroimaging assessments for patients in the TRANSEURO study. We would like to thank all the patients who took part in this study.

Funding

The research leading to these results has received funding from the European Research Council under the European Union's Seventh Framework Programme (FP7/2007–2013) [FP7–242003], from the Medical Research Council (MRC) [MR/P025870/1] and from Parkinson's UK [J-1204]. Infrastructure support for this research was provided by the NIHR Imperial Biomedical Research Centre (BRC) and NIHR Imperial CRF at Imperial College healthcare NHS trust. The views expressed are those of the authors and not necessarily those of the funder, the NHS, the NIHR, or the Department of Health. This work was also supported financially by a PhD studentship awarded to N.P.L-K from Parkinson's UK.

Competing interests

The authors report no competing interests.

References

- Abi-Dargham A, Gandelman MS, DeErausquin GA, Zea-Ponce Y, Zoghbi SS, Baldwin RM, et al. SPECT imaging of dopamine transporters in human brain with iodine-123-fluoroalkyl analogs of beta-CIT. *J Nucl Med* 1996; 37: 1129–33.
- Alvarez-Fischer D, Blessmann G, Trosowski C, Behe M, Schurrat T, Hartmann A, et al. Quantitative [(123)I]FP-CIT pinhole SPECT imaging predicts striatal dopamine levels, but not number of nigral neurons in different mouse models of Parkinson's disease. *Neuroimage* 2007; 38: 5–12.
- Bernheimer H, Birkmayer W, Hornykiewicz O, Jellinger K, Seitelberger F. Brain dopamine and the syndromes of Parkinson and Huntington. Clinical, morphological and neurochemical correlations. *J Neurol Sci* 1973; 20: 415–55.
- Calo L, Wegrzynowicz M, Santivanez-Perez J, Grazia Spillantini M. Synaptic failure and alpha-synuclein. *Mov Disord* 2016; 31: 169–77.
- Caminiti SP, Presotto L, Baroncini D, Garibotto V, Moresco RM, Gianolli L, et al. Axonal damage and loss of connectivity in nigrostriatal and mesolimbic dopamine pathways in early Parkinson's disease. *NeuroImage Clin* 2017; 14: 734–40.
- Carpenter MB, Peter P. Nigrostriatal and nigrothalamic fibers in the rhesus monkey. *J Comp Neurol* 1972; 144: 93–115.
- Castellanos G, Fernandez-Seara MA, Lorenzo-Betancor O, Ortega-Cubero S, Puigvert M, Uranga J, et al. Automated neuromelanin imaging as a diagnostic biomarker for Parkinson's disease. *Mov Disord* 2015; 30: 945–52.
- Cheng HC, Ulane CM, Burke RE. Clinical progression in Parkinson disease and the neurobiology of axons. *Ann Neurol* 2010; 67: 715–25.
- Chowdhury R, Lambert C, Dolan RJ, Duzel E. Parcellation of the human substantia nigra based on anatomical connectivity to the striatum. *Neuroimage* 2013; 81: 191–8.
- Colloby SJ, McParland S, O'Brien JT, Attems J. Neuropathological correlates of dopaminergic imaging in Alzheimer's disease and Lewy body dementias. *Brain* 2012; 135: 2798–808.
- Emond P, Garreau L, Chalon S, Boazi M, Caillet M, Bricard J, et al. Synthesis and ligand binding of nortropane derivatives: N-substituted 2beta-carbomethoxy-3beta-(4'-iodophenyl)nortropane and N-(3-iodoprop-(2E)-enyl)-2beta-carbomethoxy-3beta-(3',4'-disubstituted phenyl)nortropane. New high-affinity and selective compounds for the dopamine transporter. *J Med Chem* 1997; 40: 1366–72.
- Fabbri M, Reimao S, Carvalho M, Nunes R, Guedes L, Bouca R, et al. Substantia nigra area evaluated by neuromelanin-sensitive MRI as an imaging biomarker of disease progression in Parkinson's disease. *Eur J Neurol* 2017; 24: 485.
- Fahn S, Oakes D, Shoulson I, Kieburtz K, Rudolph A, Lang A, et al. Levodopa and the progression of Parkinson's disease. *N Engl J Med* 2004; 351: 2498–508.
- Fazio P, Svenningsson P, Cselenyi Z, Halldin C, Farde L, Varrone A. Nigrostriatal dopamine transporter availability in early Parkinson's disease. *Mov Disord* 2018; 33: 592–9.
- Fearnley JM, Lees AJ. Ageing and Parkinson's disease: substantia nigra regional selectivity. *Brain* 1991; 114 (Pt 5): 2283–301.
- Gibb WRG, Lees AJ. Anatomy, pigmentation, ventral and dorsal subpopulations of the substantia-nigra, and differential cell-death in Parkinsons-disease. *J Neurol Neurosurg Psychiatry* 1991; 54: 388–96.
- Goetz CG, Tilley BC, Shaftman SR, Stebbins GT, Fahn S, Martinez-Martin P, et al. Movement Disorder Society-sponsored revision of the Unified Parkinson's Disease Rating Scale (MDS-UPDRS): scale presentation and clinimetric testing results. *Mov Disord* 2008; 23: 2129–70.
- Guilloteau D, Emond P, Baulieu JL, Garreau L, Frangin Y, Pourcelot L, et al. Exploration of the dopamine transporter: in vitro and in vivo characterization of a high-affinity and high-specificity iodinated tropane derivative (E)-N-(3-iodoprop-2-enyl)-2beta-carbomethoxy-3beta-(4'-m ethylph enyl)nortropane (PE2I). *Nucl Med Biol* 1998; 25: 331–7.
- Gunn R, Coello C, Searle G. Molecular Imaging And Kinetic Analysis Toolbox (MIKAT) - A quantitative software package for the analysis of PET neuroimaging data. *J Nuclear Med* 2016; 57 (Suppl 2): 1928.
- Guttman M, Stewart D, Hussey D, Wilson A, Houle S, Kish S. Influence of L-dopa and pramipexole on striatal dopamine transporter in early PD. *Neurology* 2001; 56: 1559–64.
- Haber SN. The place of dopamine in the cortico-basal ganglia circuit. *Neuroscience* 2014; 282: 248–57.
- Haber SN, Fudge JL, McFarland NR. Striatonigrostriatal pathways in primates form an ascending spiral from the shell to the dorsolateral striatum. *J Neurosci* 2000; 20: 2369–82.
- Hall H, Halldin C, Guilloteau D, Chalon S, Emond P, Besnard J, et al. Visualization of the dopamine transporter in the human brain post-mortem with the new selective ligand [125I]PE2I. *Neuroimage* 1999; 9: 108–16.
- Halldin C, Erixon-Lindroth N, Pauli S, Chou YH, Okubo Y, Karlsson P, et al. [(11)C]PE2I: a highly selective radioligand for PET examination of the dopamine transporter in monkey and human brain. *Eur J Nucl Med Mol Imaging* 2003; 30: 1220–30.
- Han S, Oh M, Oh JS, Lee SJ, Oh SJ, Chung SJ, et al. Subregional pattern of striatal dopamine transporter loss on 18F FP-CIT positron emission tomography in patients with pure akinesia with gait freezing. *JAMA Neurol* 2016; 73: 1477–84.
- Harrell FE Jr. Hmisc: Harrell Miscellaneous. R package version 4.0–3. 2017. <https://CRAN.R-project.org/package=Hmisc>.
- Hughes AJ, Daniel SE, Kilford L, Lees AJ. Accuracy of clinical diagnosis of idiopathic Parkinson's disease: a clinico-pathological study of 100 cases. *J Neurol Neurosurg Psychiatry* 1992; 55: 181–4.
- Isaias IU, Trujillo P, Summers P, Marotta G, Mainardi L, Pezzoli G, et al. Neuromelanin imaging and dopaminergic loss in Parkinson's disease. *Front Aging Neurosci* 2016; 8: 196.
- Ishibashi K, Ishii K, Oda K, Kawasaki K, Mizusawa H, Ishiwata K. Regional analysis of age-related decline in dopamine transporters and dopamine D2-like receptors in human striatum. *Synapse* 2009; 63: 282–90.
- Ito H, Kawaguchi H, Kodaka F, Takuwa H, Ikoma Y, Shimada H, et al. Normative data of dopaminergic neurotransmission functions in substantia nigra measured with MRI and PET: Neuromelanin,

- dopamine synthesis, dopamine transporters, and dopamine D2 receptors. *Neuroimage* 2017; 158: 12–7.
- Jenkinson M, Beckmann CF, Behrens TE, Woolrich MW, Smith SM. *Fsl. Neuroimage* 2012; 62: 782–90.
- Jucaite A, Odano I, Olsson H, Pauli S, Halldin C, Farde L. Quantitative analyses of regional [11C]PE2I binding to the dopamine transporter in the human brain: a PET study. *Eur J Nucl Med Mol Imaging* 2006; 33: 657–68.
- Kashihara K, Shinya T, Higaki F. Neuromelanin magnetic resonance imaging of nigral volume loss in patients with Parkinson's disease. *J Clin Neurosci* 2011; 18: 1093–6.
- Kish SJ, Shannak K, Hornykiewicz O. Uneven pattern of dopamine loss in the striatum of patients with idiopathic Parkinson's-Disease - pathophysiologic and clinical implications. *N Engl J Med* 1988; 318: 876–80.
- Kitao S, Matsusue E, Fujii S, Miyoshi F, Kaminou T, Kato S, et al. Correlation between pathology and neuromelanin MR imaging in Parkinson's disease and dementia with Lewy bodies. *Neuroradiology* 2013; 55: 947–53.
- Kordower JH, Olanow CW, Dodiya HB, Chu Y, Beach TG, Adler CH, et al. Disease duration and the integrity of the nigrostriatal system in Parkinson's disease. *Brain* 2013; 136: 2419–31.
- Kraemmer J, Kovacs GG, Perju-Dumbrava L, Pirker S, Traub-Weidinger T, Pirker W. Correlation of striatal dopamine transporter imaging with post mortem substantia nigra cell counts. *Mov Disord* 2014; 29: 1767–73.
- Kurowska Z, Kordower JH, Stoessl AJ, Burke RE, Brundin P, Yue ZY, et al. Is Axonal Degeneration a Key Early Event in Parkinson's Disease? *J Parkinson Dis* 2016; 6: 703–7.
- Kuya K, Shinohara Y, Miyoshi F, Fujii S, Tanabe Y, Ogawa T. Correlation between neuromelanin-sensitive MR imaging and I-123-FP-CIT SPECT in patients with parkinsonism. *Neuroradiology* 2016; 58: 351–6.
- Lammertsma AA, Hume SP. Simplified reference tissue model for PET receptor studies. *Neuroimage* 1996; 4: 153–8.
- Lee CS, Samii A, Sossi V, Ruth TJ, Schulzer M, Holden JE, et al. In vivo positron emission tomographic evidence for compensatory changes in presynaptic dopaminergic nerve terminals in Parkinson's disease. *Ann Neurol* 2000; 47: 493–503.
- Lenth RV. emmeans: Estimated Marginal Means, aka Least-Squares Means. R package version 1.2.3. 2018. <https://CRAN.R-project.org/package=emmeans>.
- Li W, Lao-Kaim NP, Roussakis AA, Martín-Bastida A, Valle-Guzman N, Paul G, et al. (11) C-PE2I and (18) F-Dopa PET for assessing progression rate in Parkinson's: a longitudinal study. *Mov Disord* 2018; 33: 117–27.
- Lynd-Balta E, Haber SN. The organization of midbrain projections to the striatum in the primate: sensorimotor-related striatum versus ventral striatum. *Neuroscience* 1994; 59: 625–40.
- Matsuura K, Maeda M, Yata K, Ichiba Y, Yamaguchi T, Kanamaru K, et al. Neuromelanin magnetic resonance imaging in Parkinson's disease and multiple system atrophy. *Eur Neurol* 2013; 70: 70–7.
- Mazziotta JC, Toga AW, Evans A, Fox P, Lancaster J. A probabilistic atlas of the human brain: theory and rationale for its development. The International Consortium for Brain Mapping (ICBM). *Neuroimage* 1995; 2: 89–101.
- Nandhagopal R, Kuramoto L, Schulzer M, Mak E, Cragg J, Lee CS, et al. Longitudinal progression of sporadic Parkinson's disease: a multi-tracer positron emission tomography study. *Brain* 2009; 132: 2970–9.
- Nyberg P, Nordberg A, Wester P, Winblad B. Dopaminergic deficiency is more pronounced in putamen than in nucleus caudatus in Parkinson's disease. *Neurochem Pathol* 1983; 1: 193–202.
- Ogisu K, Kudo K, Sasaki M, Sakushima K, Yabe I, Sasaki H, et al. 3D neuromelanin-sensitive magnetic resonance imaging with semi-automated volume measurement of the substantia nigra pars compacta for diagnosis of Parkinson's disease. *Neuroradiology* 2013; 55: 719–24.
- Oh M, Kim JS, Kim JY, Shin KH, Park SH, Kim HO, et al. Subregional patterns of preferential striatal dopamine transporter loss differ in Parkinson disease, progressive supranuclear palsy, and multiple-system atrophy. *J Nucl Med* 2012; 53: 399–406.
- Ohtsuka C, Sasaki M, Konno K, Koide M, Kato K, Takahashi J, et al. Changes in substantia nigra and locus coeruleus in patients with early-stage Parkinson's disease using neuromelanin-sensitive MR imaging. *Neurosci Lett* 2013; 541: 93–8.
- R Core Team. R: A language and environment for statistical computing. Vienna, Austria. 2017. <https://www.R-project.org/>.
- Reimao S, Pita Lobo P, Neutel D, Correia Guedes L, Coelho M, Rosa MM, et al. Substantia nigra neuromelanin magnetic resonance imaging in de novo Parkinson's disease patients. *Eur J Neurol* 2015; 22: 540–6.
- Saari L, Kivinen K, Gardberg M, Joutsa J, Noponen T, Kaasinen V. Dopamine transporter imaging does not predict the number of nigral neurons in Parkinson disease. *Neurology* 2017; 88: 1461–7.
- Sasaki M, Shibata E, Tohyama K, Takahashi J, Otsuka K, Tsuchiya K, et al. Neuromelanin magnetic resonance imaging of locus ceruleus and substantia nigra in Parkinson's disease. *Neuroreport* 2006; 17: 1215–8.
- Scherman D, Desnos C, Darchen F, Pollak P, Javoy-Agid F, Agid Y. Striatal dopamine deficiency in Parkinson's disease: role of aging. *Ann Neurol* 1989; 26: 551–7.
- Schwarz ST, Rittman T, Gontu V, Morgan PS, Bajaj N, Auer DP. T1-weighted MRI shows stage-dependent substantia nigra signal loss in Parkinson's disease. *Mov Disord* 2011; 26: 1633–8.
- Seibyl JP, Marek KL, Quinlan D, Sheff K, Zoghbi S, Zea-Ponce Y, et al. Decreased single-photon emission computed tomographic [123I]beta-CIT striatal uptake correlates with symptom severity in Parkinson's disease. *Ann Neurol* 1995; 38: 589–98.
- Shingai Y, Tateno A, Arakawa R, Sakayori T, Kim W, Suzuki H, et al. Age-related decline in dopamine transporter in human brain using PET with a new radioligand [F-18]FE-PE2I. *Ann Nucl Med* 2014; 28: 220–6.
- Singmann H, Bolker B, Westfall J, Aust F. afex: Analysis of Factorial Experiments. R package version 0.18–0. 2017. <https://CRAN.R-project.org/package=afex>.
- Sulzer D, Cassidy C, Horga G, Kang UJ, Fahn S, Casella L, et al. Neuromelanin detection by magnetic resonance imaging (MRI) and its promise as a biomarker for Parkinson's disease. *NPJ Parkinson's Dis* 2018; 4: 11.
- Szabo J. Organization of the ascending striatal afferents in monkeys. *J Comp Neurol* 1980; 189: 307–21.
- Tagliaferro P, Burke RE. Retrograde Axonal Degeneration in Parkinson Disease. *J Parkinsons Dis* 2016; 6: 1–15.
- Tomlinson CL, Stowe R, Patel S, Rick C, Gray R, Clarke CE. Systematic review of levodopa dose equivalency reporting in Parkinson's disease. *Mov Disord* 2010; 25: 2649–53.
- Tziortzi AC, Searle GE, Tzimopoulou S, Salinas C, Beaver JD, Jenkinson M, et al. Imaging dopamine receptors in humans with [11C](+)-PHNO: dissection of D3 signal and anatomy. *Neuroimage* 2011; 54: 264–77.
- Xing Y, Sapuan A, Dineen RA, Auer DP. Life span pigmentation changes of the substantia nigra detected by neuromelanin-sensitive MRI. *Mov Disord* 2018; 33: 1792–9.
- Zecca L, Zucca FA, Albertini A, Rizzio E, Fariello RG. A proposed dual role of neuromelanin in the pathogenesis of Parkinson's disease. *Neurology* 2006; 67: S8–S11.
- Zucca FA, Basso E, Cupaioli FA, Ferrari E, Sulzer D, Casella L, et al. Neuromelanin of the human substantia nigra: an update. *Neurotox Res* 2014; 25: 13–23.
- Zucca FA, Segura-Aguilar J, Ferrari E, Munoz P, Paris I, Sulzer D, et al. Interactions of iron, dopamine and neuromelanin pathways in brain aging and Parkinson's disease. *Prog Neurobiol* 2017; 155: 96–119.